

Organic Surface Chemistry

Approach Matters: The Kinetics of Interfacial Inverse-Electron Demand Diels–Alder Reactions

Rickdeb Sen^{+, [a]}, Digvijay Gahtory^{+, [a]}, Jorge Escorihuela,^[a] Judith Firet,^[a] Sidharam P. Pujari,^[a] and Han Zuilhof^{*, [a, b, c]}

Dedicated to Dr. Gerrit Lodder on the occasion of his 77th birthday

Abstract: Rapid and quantitative click functionalization of surfaces remains an interesting challenge in surface chemistry. In this regard, inverse electron demand Diels–Alder (IEDDA) reactions represent a promising metal-free candidate. Herein, we reveal quantitative surface functionalization within 15 min. Furthermore, we report the comprehensive effects of substrate stereochemistry, surrounding microenvironment and substrate order on the reaction kinetics as obtained by surface-bound mass spectrometry (DART-HRMS).

The excellent kinetics, high yields, lack of by-products and high stereoselectivity of click reactions have led to their extensive use in total synthesis,^[1] and biorthogonal^[2] and site-specific^[3,4] labelling of biomolecules. The utility of these reactions for surface modification has blossomed in recent times as evident from a significant number of reports,^[5] specifically their use in biomolecular attachment and patterning.^[6] Crucial for surface modification are the rate of reactions (for effective implementation) and complete conversion of the surface-bound moiety to the product of interest. The latter aspect is of importance, as surface-bound moieties cannot be removed afterwards by

the standard purifications techniques so central to solution-phase chemistry (column chromatography, HPLC, etc.).

In these regards, the inverse electron demand Diels–Alder reaction (IEDDA) between 1,2,4,5-tetrazine and strained alkenes/alkynes holds great promise.^[7] IEDDA reactions have been extensively studied in solution with particular focus on tuning the steric and electronic effects of a wide variety of dienes and dienophiles.^[8] Such studies indicated very interesting features such as very fast reaction kinetics^[8a,9] (among the highest for metal-free click reactions) and high chemoselectivity. Surprisingly, this facile reaction has been largely underexplored for surface functionalization with a few examples in literature using the highly reactive, but somewhat unstable *trans*-cyclooctene (TCO) reacting with tetrazine,^[2,10] or a more stable but less reactive reactant such as norbornene.^[11] In studies of click reactions at surface, both metal-catalyzed and metal-free a recurring but hitherto largely unresolved issue is the question whether it matters which component is better to be surface-bound or better to be in solution, that is, in this case norbornene_(surf.) + tetrazine_(soln.) versus tetrazine_(surf.) + norbornene_(soln.). For example, for both interfacial strain-promoted azide–alkyne cycloadditions^[12] and surface-bound thiol–ene click reactions^[13] the choice of the surface-bound reaction partner, that is, overall reaction orientation, is important, but published results are inconclusive in this regard.

We have recently shown that the microenvironment around the reactive site on the surface plays an important role in the kinetics of strain-promoted click reactions, as determined by highly accurate and facile rate studies using direct analysis in real time-high resolution mass spectrometry (DART-HRMS).^[14] Those studies allowed and stimulated us to investigate whether the microenvironment for the interfacial IEDDA using the more stable norbornene could be optimized to further improve the reaction rates, and possibly direct the yield of surface-bound IEDDA reactions towards 100%.

Given the high signal/noise (S/N) ratio of DART-HRMS, for example: about two orders of magnitude better than X-ray photoelectron spectroscopy (XPS), we are in this study for the first time able to systematically tune three aspects relevant for surface-bound organic conversions in detail (Scheme 1): surface-induced sterics (are the groups buried in a monolayer, or sticking out above it), stereochemistry (*endo/exo*-norbornene, as a means to investigate the effects of approach of the reactant in solution) and orientation (which reactant is in the solvent and which one surface-bound).^[15] Optimization of these factors

[a] R. Sen,⁺ D. Gahtory,⁺ Dr. J. Escorihuela, J. Firet, Dr. S. P. Pujari, Prof. Dr. H. Zuilhof
Laboratory of Organic Chemistry
Wageningen University and Research, Stippeneng 4
6708 WE Wageningen (The Netherlands)

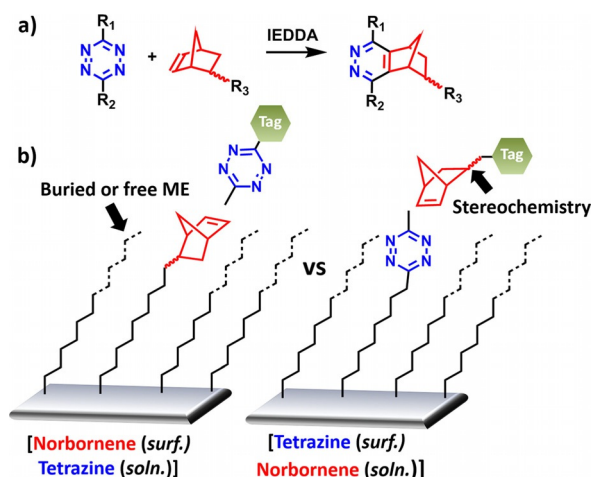
[b] Prof. Dr. H. Zuilhof
School of Pharmaceutical Sciences and Technology
Tianjin University, 92 Weijin Road, Tianjin (P.R. China)

[c] Prof. Dr. H. Zuilhof
Department of Chemical and Materials Engineering
King Abdulaziz University, Jeddah (Saudi Arabia)
E-mail: han.zuilhof@wur.nl

[†] These authors contributed equally to this work.

Supporting information and the ORCID identification numbers for the authors of this article can be found under <https://doi.org/10.1002/chem.201703103>.

© 2017 The Authors. Published by Wiley-VCH Verlag GmbH & Co. KGaA. This is an open access article under the terms of Creative Commons Attribution NonCommercial-NoDerivs License, which permits use and distribution in any medium, provided the original work is properly cited, the use is non-commercial and no modifications or adaptations are made.



Scheme 1. a) Overall tetrazine-norbornene IEDDA reaction and b) schematic depicting the three parameters (in parentheses) under current study.

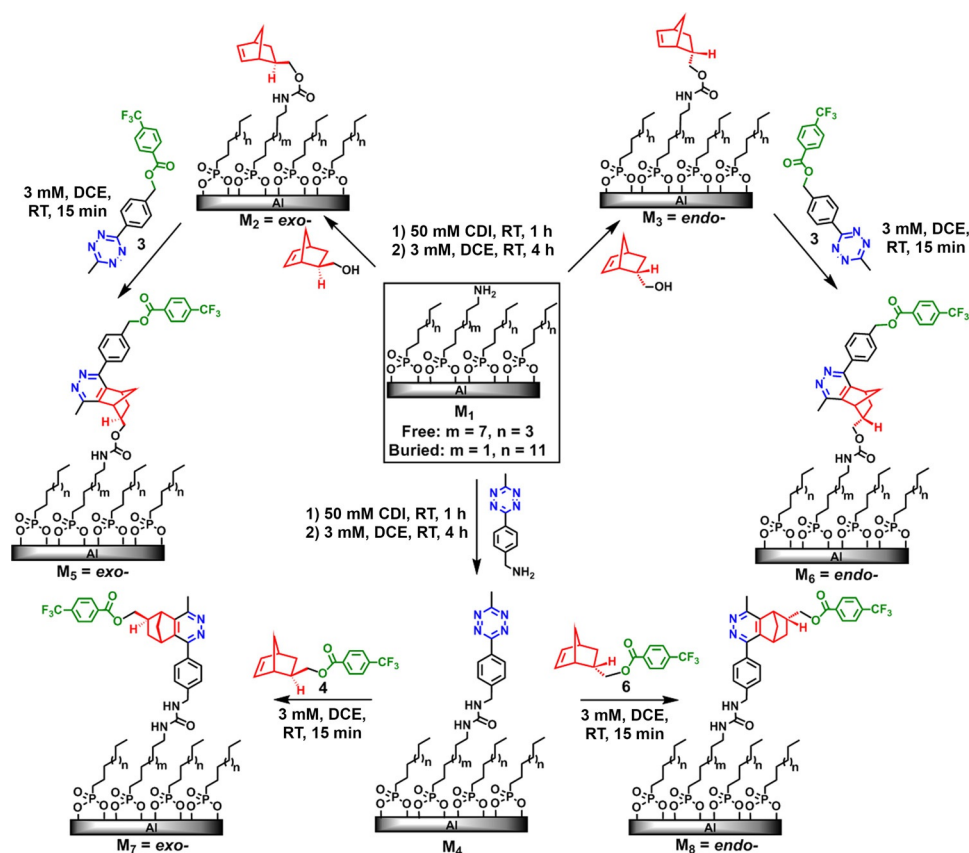
yielded conditions in which the reaction is quantitative and complete within 15 minutes, showing the potential of both this systematic approach and of this reaction.

To this end, first the surface of aluminum (Al) slides with its natural aluminum oxide coating were covalently modified by phosphonic acid-based monolayers via a well-established methodology.^[5a] For this study, we prepared 3:1 alkyl to amine-terminated monolayers (M_1 ; see Scheme 2), as previous studies indicated this to be the optimum between high density of

functionalization and reactivity. In our experience, increasing the dilution of the reactive sites in the monolayers higher than 33% leads to overall decreased reaction kinetics and reaction yields.^[14] The microenvironment of the reacting groups was tuned by modifying the lengths of the surrounding alkyl chains, so as to bury it in the monolayer (4 carbon atoms below the surface), or make it stick out (4 carbon atoms above the surface). The monolayer composition was confirmed by the N/P ratio (1:4) in XPS wide scans (Figure S5.1 in the Supporting Information). In order to obtain a better understanding of surface coverage, a molecular mechanics study was performed that studied the average packing energy per chain in dependence of the packing density.^[16] This was performed by creating schematic models of varying degrees of alkyl monolayer attachment with different random attachment at the available sites followed by optimization of the corresponding molecular models.

For more detailed understanding of the randomization process, see sections 7.1–7.9 in the Supporting Information. We found that roughly 50% coverage corresponded to the lowest packing energy per molecule (Supporting Information, sections 7.10 and 7.11). This means that ideally about half the surface sites available result in monolayer attachment.

Norbornene surfaces (M_2/M_3) were prepared by coupling 5-norbornene-2-methanol (*exo*-/*endo*-) to M_1 surfaces by a carbamate linkage (Scheme 2 and Figure S4.4, S5.2 and S5.3). For preparation of tetrazine surfaces (M_4), we chose unsymmetrical tetrazine with benzyl amine and methyl substitution, again via



Scheme 2. General scheme for the surface modification followed by interfacial IEDDA reaction.

a carbamate linkage to ensure the same freedom/buried nature as in M_2/M_3 . As shown by the groups of Hilderbrand and Chen, unsymmetrical tetrazines provide a better balance between stability and reactivity than their symmetric counterparts,^[6b,17] while also ensuring enough rigidity on a surface. Complete surface attachment for M_4 surfaces was obtained for this reaction as confirmed by N/P ratios (1.5 ± 0.1) in XPS analysis (Figure S5.4 in the Supporting Information). After confirmation of surface attachment of norbornenes and tetrazines, respectively, we embarked on exploring the IEDDA reaction. For easy analysis of the reaction progress, we synthesized compounds with fluorinated tags **3**, **4** and **6** that facilitate analysis by both XPS and DART-HRMS. The reactions were performed for both the reaction partners under stringently similar conditions (Scheme 2) and followed by monitoring the F/P ratio in XPS wide spectra (Figure 1). Interestingly, we found that for the “free” M_2 , M_3 and M_4 systems, a quantitative surface reaction yield was obtained within 15 min irrespective of the orientation of the reaction (Figure S5.5 and S5.6 in the Supporting Information). In case of the “buried” system, the crowded microenvironments around the reactive sites slowed the reaction down, yielding a slightly lower reaction yield ($\approx 80\%$) after 15 min for “buried” exo -norbornene_(surf.) + tetrazine_(soln.) system (Figure S5.10), but $>90\%$ conversion was also observed for such crowded microenvironments after 1 h (Figure S5.11). See the Supporting Information for a more detailed description of the different calculations used for reaction quantification using XPS wide and narrow spectra.

To obtain accurate reaction kinetics, we reacted our samples for different time intervals (up to 20 min) and followed the signal intensity of the corresponding MS-tag (m/z 189.016) in DART-HRMS. Using such high S/N data, the pseudo-first order rate constant (k) was calculated as the slope of the plot of $\ln|(I_t - I_\infty)/(I_0 - I_\infty)|$ versus time (t), in which I_∞ corresponds to the asymptotic integrated extracted ion chromatogram (EIC) intensity at obtained by exponential decay curve fitting of the data (Supporting Information, Figure S3.1–S3.8); the second-order rate constants were derived from there. The highest second-order reaction rate constant ($3.62 \text{ M}^{-1} \text{ s}^{-1}$ at a solute concentration of 3.0 mM , 30°C , 1,2-dichloroethane (DCE)) was observed for exo -norbornene_(surf.) with tetrazine_(soln.) **3** in a “free”

microenvironment (Figure 2). Using the inverse situation, tetrazine on a surface surrounded by lower alkyl chains reacting with exo -norbornene **4** in solution, afforded a two-fold slower rate (Figure 2).

The IEDDA reaction efficiency can be determined by comparing the atomic ratio determined by XPS with the theoretical value of 3:4 (for F/P), which corresponds to the 100% surface conversion. Interestingly, recently we reported the first 100%-yielding surface-bound metal-free click reaction (a strain-promoted cyclooctyne–quinone or SPOCQ reaction), which was further characterized by a second order rate constant (k') of $3.3 \text{ M}^{-1} \text{ s}^{-1}$.^[14a] While thus displaying virtually the same rate, in

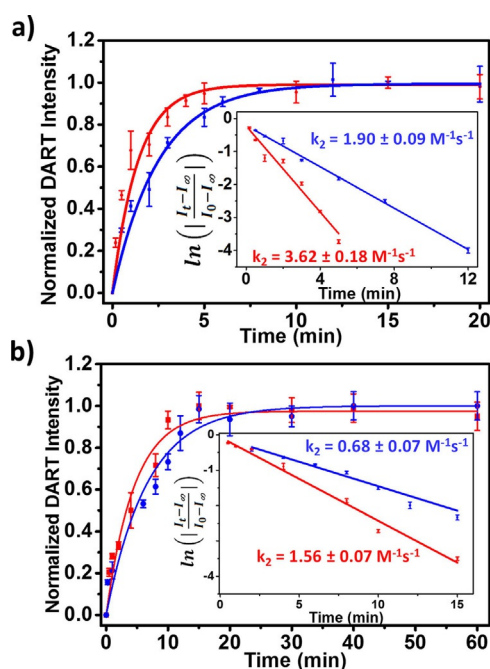


Figure 2. Normalized DART-HRMS intensity vs. time (min) for IEDDA in a “free” microenvironment: a) exo -Norbornene surfaces (M_2) reacting with **3** (red) and tetrazine surfaces (M_4) reacting with **4** (blue). b) $endo$ -Norbornene surfaces (M_3) reacting with **3** (red) and tetrazine surfaces (M_4) reacting with **6** (blue). Inserts: Linear plots of $\ln[(I_t - I_\infty)/(I_0 - I_\infty)]$ versus time (min) to obtain the pseudo-first order constants, and using solute concentrations of 3.0 mM the subsequently derived 2nd order rate constants (k_2).

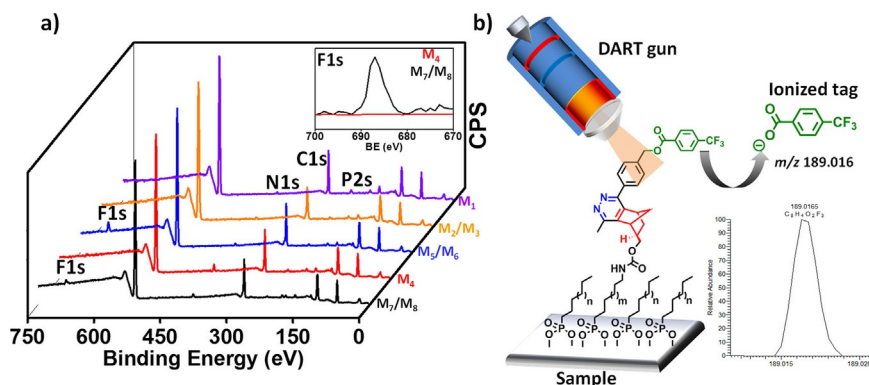


Figure 1. a) XPS wide range spectra for M_1 – M_8 surfaces showing emergence of F1s signal after the interfacial IEDDA reaction. b) Schematic impression of ionization of MS-tag (m/z 189.0163) by DART-HRMS.

that case, we observed two distinct kinetic regimes: an initial fast regime followed by a slower, more complex one; the rate constant refers to the initial well-behaved kinetic regime only. The SPOCQ reaction was eventually also quantitative, but reaches full conversion only in 4 h. Here, the IEDDA reaction turned out to be a significant improvement, reaching an unprecedented complete conversion within 15 minutes, while the entire kinetic regime could be followed using one exponent, that is, the IEDDA reaction displays clean kinetics.

In addition, excellent yields were obtained both in “free” and “buried” conditions, and independent of the orientation of the reaction, thereby showing the scope of this strategy for surface modifications. Changing the stereochemistry of the immobilized norbornene to *endo*- in a “free” microenvironment halved the reaction rate (Figure S3.3) which is consistent with the rate differences observed in solution.^[9b] Interestingly, also in this case a kinetic preference (two-fold difference) was observed for immobilized norbornene reacting with tetrazine in solution than its reverse, that is, tetrazine on the surface reacting with *endo*-norbornene **6** in solution (Table 1). This result outlines that the slowing down of reaction rate for tetrazine immobilization occurs irrespective of norbornene stereochemistry.

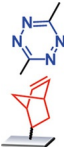
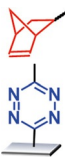
Finally, we wanted to know the kinetic effects of doing the reaction “above” the monolayer versus “within” the monolayer. Therefore we studied the reaction in a “buried” state: surfaces were prepared with either norbornene or tetrazine moieties bound to the surface that are surrounded by long alkyl chains, and used for IEDDA reaction (Scheme 2). The rate differences again amounted to about two folds in favor of norbornene immobilization (Table 1). The highest reaction rate in this microenvironment ($0.87 \text{ M}^{-1} \text{ s}^{-1}$) was observed for *exo*-norbornene attached on the surface reacting with tetrazine and the lowest ($0.58 \text{ M}^{-1} \text{ s}^{-1}$) was observed for its reverse. Comparing the best and worst possibility, the rate constant for the *exo*-norbornene immobilization in “free” microenvironment was 6.2 fold higher than that for tetrazine immobilization in a “buried” state. It is of relevance to state that only with high S/N-techniques like

DART-HRMS such relatively small rate differences can come into view and thus be rationalized.

To this latter aim, we also applied quantum chemical and molecular mechanics calculations. The reaction between unsubstituted^[18] and substituted tetrazines^[19] and various alkenes has been studied theoretically by Houk, Devaraj, and co-workers. In our case, we modeled the IEDDA reaction between a substituted tetrazine and *exo*-/*endo*-norbornene (substituted so as to mimic their surface attachment or solution functionalities, see Figure 3). In line with previous findings, density functional theory (DFT) calculations (at M06-2X/6-311+G(d,p) level) revealed that the Diels–Alder cycloaddition, rather than the subsequent N_2 expulsion, is the rate-determining step in this reaction. In accordance with experimental results, *exo*-norbornene has a lower activation barrier than *endo*-norbornene (Figure 3a). Also, our calculations show that the reaction corresponding to norbornene_(surf.) (*exo*- and *endo*-) and tetrazine_(soln.) had a lower energy barrier (by $\approx 1 \text{ kcal mol}^{-1}$) than the reverse orientation (Figure 3b,c). This energy difference is in line with the observed rate difference for the interfacial IEDDA in the “free” microenvironment.

A visual representation of the orientation of immobilized groups was obtained by performing sequential molecular dynamics and molecular mechanics optimizations of the IEDDA cycloadducts on aluminum oxide surface. The modelling was performed on large supercells obtained by attachment of the norbornene or tetrazine moieties in a random pattern followed by subsequent energy minimization (see section 7.13–7.14 in the Supporting Information). Next, a series of molecular dynamics runs at 773.0 K was performed to “shake up” the conformations of the chains, and get truly random orientations of the surface-bound moieties. Finally, those geometries were optimized by molecular mechanics, to indicate the most stable orientations of reactive groups with respect to the surface (see section 7.15–7.19 in the Supporting Information and two movies with rotating 3D structures of the surface). Representative geometries, from a much large set, are shown in Figure 4. For surface-bound norbornenes (Figure 4a), the surface-bound

Table 1. Second-order rate constants k_2 [$\text{M}^{-1} \text{s}^{-1}$] of the tetrazine-norbornene IEDDA reaction in “free” and “buried” microenvironments.

Surface group		Reactant in solution		
norbornene		free	$3.62 \pm 0.18 \text{ M}^{-1} \text{ s}^{-1}$ (<i>exo</i> -)	$1.56 \pm 0.07 \text{ M}^{-1} \text{ s}^{-1}$ (<i>endo</i> -)
		buried	$0.87 \pm 0.06 \text{ M}^{-1} \text{ s}^{-1}$ (<i>exo</i> -)	$0.57 \pm 0.08 \text{ M}^{-1} \text{ s}^{-1}$ (<i>endo</i> -)
		free	$1.90 \pm 0.09 \text{ M}^{-1} \text{ s}^{-1}$ (<i>exo</i> -)	$0.68 \pm 0.07 \text{ M}^{-1} \text{ s}^{-1}$ (<i>endo</i> -)
		buried	$0.58 \pm 0.08 \text{ M}^{-1} \text{ s}^{-1}$ (<i>exo</i> -)	$0.61 \pm 0.05 \text{ M}^{-1} \text{ s}^{-1}$ (<i>endo</i> -)

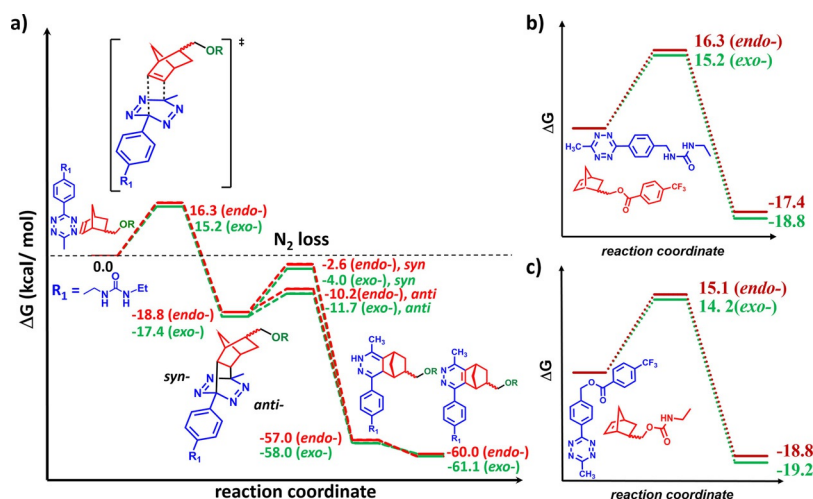


Figure 3. a) DFT calculation for the full mechanism of the multistep IEDDA reaction between an unsymmetrical tetrazine and *exo*- and *endo*-norbornene mimicking molecules used in our work, b,c) reaction coordinate diagram for the IEDDA reaction mimicking our reaction condition showing tetrazine and *exo*-/*endo*-norbornene on surface, respectively.

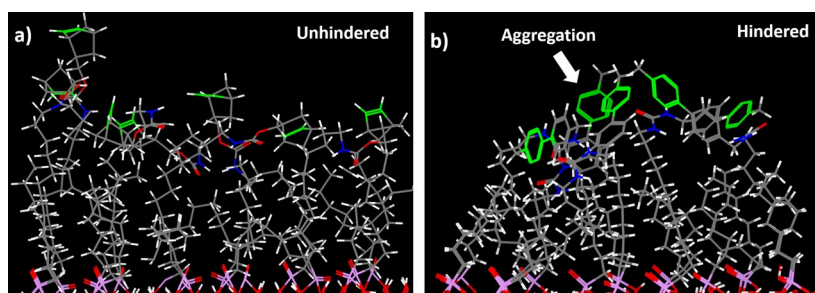


Figure 4. Comparison of surface disposition of IEDDA reactants in “free” ME after molecular dynamics of: a) norbornene_(surf.) and b) tetrazine_(surf.).

molecules prefer to be apart (no specific attractions; significant steric repulsions) with the double bond (highlighted in green) facing outwards. In contrast, tetrazines_(surf.) in a “free” microenvironment showed a higher propensity to clump/cluster together due to additional stabilization attributable to π - π stacking (Figure 4b). These orientations and clustering (or lack thereof) will influence the reactivity and angle of approach of any reacting solute.

Based on the transition-state geometry obtained by DFT calculations we deduce that the approach of tetrazine_(soln.) moieties preferentially occurs in a “top-down” manner or perpendicular to the surface (Figure 5a). In contrast, the approach of the incoming norbornene_(soln.) should be side-ways or parallel to the surface (Figure 5b), and the reactant in solution thus encounters a lot more steric hindrance along the reaction path. In addition, the aggregation of surface-bound tetrazines also lowers the available number of tetrazines in statistical terms by masking one or both the available faces. Both these factors will likely contribute to the overall slower kinetics of tetrazine_(surf.) + norbornene_(soln.) reaction. These findings point to the overall relevance of choosing prior to immobilization which agent is surface-bound and which comes in from solution.

In conclusion, we have achieved an expeditious (within 15 min) and quantitative surface functionalization using inverse

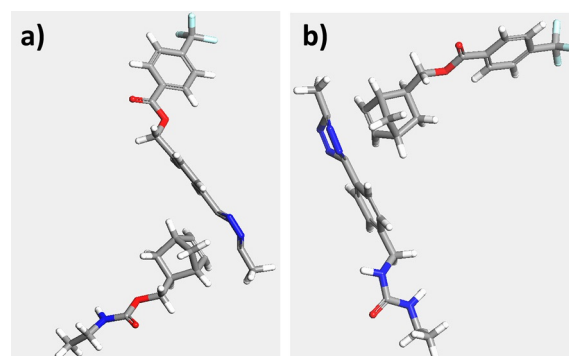


Figure 5. DFT calculation of approach of: a) norbornene_(surf.) with tetrazine_(soln.) and b) vice-versa, clearly showing different angles of approach to surface groups.

electron demand Diels–Alder reactions. The reaction displays clean pseudo-first order kinetics over the full conversion range. We found that the approach of the solution reactant towards the surface-bound counterpart plays an important role in the course of the reaction, supporting the significance of the orientation in surface-bound reactions. Such detailed insights into surface-bound organic reactions are both required and becoming available by combining techniques like XPS and DART-

MS to further improve surface modification procedures for a wide range of applications.

Experimental Section

Materials

Unless otherwise specified, all chemicals were used as received without further purification. Octylphosphonic acid, hexadecylphosphonic acid, 1,1'-carbonyldiimidazole (CDI), *exo*-5-norbornene-2-methanol, hydrochloric acid, methanol, hexane, acetone, dichloromethane (CH₂Cl₂), 1,2-dichloroethane (DCE) and 2-propanol were purchased from Sigma-Aldrich. 12-Aminododecylphosphonic acid hydrochloride salt and 6-aminohexylphosphonic acid hydrochloride salt were purchased from SIKÉMIA. Aluminium pieces (99.5% purity, mirror polished, Staalmarkt Beuningen BV) were cut using mechanical cutter into exactly 2×1 cm dimension. For surface modification reactions, the samples were loaded onto a specially constructed PTFE wafer holder able to hold up to 16 samples at a time thus ensuring rigorous reproducibility between samples.

X-ray photoelectron spectroscopy (XPS) measurements

The XPS analysis of surfaces was performed using a JPS-9200 photoelectron spectrometer (JEOL, Japan). Survey and high-resolution spectra were obtained under UHV conditions using monochromatic AlK α X-ray radiation at 12 kV and 20 mA, and an analyzer pass energy of 50 eV for wide scans and 10 eV for narrow scans. The emitted electrons were collected at 10° from the surface normal (take-off angle relative to the surface normal 10°). All XPS spectra were evaluated by using Casa XPS software (version 2.3.15). Survey spectra were corrected with linear background before fitting, whereas high-resolution spectra were corrected with linear background. Atomic area ratios were determined after a baseline correction and normalizing the peak area ratios by the corresponding atomic sensitivity factors (1.00 for C1s, 1.80 for N1s, 2.93 for O1s, 4.43 for F1s, 1.18 for P2s and 0.75 for Al2s).

DART-HRMS measurements

Analysis of the modified mica surfaces were performed using a DART-SVP ion source (Ion-Sense, Saugus, MA, USA) coupled to a Q-Exactive orbitrap high-resolution mass spectrometer (Thermo Fisher Scientific, San Jose, CA, USA), mounted on a motorized rail travelling at 0.2 mm s⁻¹. Thermo Scientific Xcalibur software (V2.1.0.1139) was used for data acquisition and processing. The measurements were performed in negative mode at 450 °C using a scan range of *m/z* 188.6–189.4, a mass resolution of 70 000 (FWHM) at a scan rate of 1 Hz. The ion trap was tuned with 0.1 mg mL⁻¹ methanol solution of quinine (*m/z* 323.41 in negative mode) and optimized. The DART source was positioned 6.1 cm on the horizontal scale, 7 cm on the vertical scale with an angle of 45°, such that it is around 1 mm above the surface (Figure S4.1). The distance from the surface to the ceramic tube is minimized by placing them at the edge of the moving rail so that maximum of the (4-trifluoro)methyl benzoate ion (*m/z* 189.016 respectively) would enter the MS.^[14]

Computational procedures

All of the DFT calculations reported herein were carried out using Gaussian09.^[20] All geometries were fully optimized using the M06-2X functional^[21] and the 6-311+G (d,p) basis set, which has been found to give relatively accurate energetics for cycloadditions.^[18,22]

Analytical frequencies were calculated at this level in all cases, and the nature of the stationary points was determined in each case according to the proper number of imaginary frequencies. The intrinsic reaction coordinate (IRC) path was traced to check the energy profiles connecting each transition state to the two associated minima of the proposed mechanism.^[23] Initially, a Monte Carlo conformational search using conformer distribution option available in Spartan'14 was used (Wavefunction, Inc., Irvine, CA, USA, 2014). With this option, a search without constraints was performed for every structure. The torsion angles were randomly varied and the obtained structures were fully optimized using the MMFF force field. Thus, different minima of energy within an energy gap of 10 kcal mol⁻¹ were generated. These structures were analyzed and ordered considering the relative energy, being the repeated geometries eliminated. In all cases, molecules with the lowest energy and an energy gap of 4.0 kcal mol⁻¹ were selected and studied quantum chemically.

Synthesis of 3-methyl-6-phenyl methylamine-1,2,4,5-tetrazine (1)

Metal-catalyzed tetrazine synthesis described elsewhere^[24] was applied to synthesize 3-methyl-6-phenyl methylamine-1,2,4,5-tetrazine. Briefly, 4-(aminomethyl)benzotrile hydrochloride (1.50 g, 8.9 mmol), Ni(OTf)₂ (1.59 g, 4.45 mmol), and acetonitrile (4.7 mL, 89 mmol) were added in a 250 mL round flask, followed adding 60% NH₂NH₂·H₂O (30 mL), under N₂ flow. The mixture was stirred at 60 °C for 16 h and allowed to cool to room temperature. Sodium nitrite (14.6 g, 212 mmol) in 25 mL of water was slowly added to the reaction followed by 5 M HCl until gas evolution ceased (pH 3), in an ice bath. The product was extracted into ethyl acetate and purified by silica column chromatography (MeOH:CH₂Cl₂ = 1:9) as a red solid. Yield: 0.56 g (27%). ¹H NMR (400 MHz, [D₆]DMSO): δ = 2.99 (3H, s), 4.15 (2H, s), 7.71 (2H, d, *J* = 8 Hz), 8.49 ppm (2H, d, *J* = 8 Hz); ¹³C NMR (101 MHz, [D₆]DMSO): δ = 20.8, 42.3, 127.6, 129.5, 131.8, 139.2, 162.3, 167.2 ppm.

Synthesis of 3-methyl-6-phenyl methanol-1,2,4,5-tetrazine (2)

3-Methyl-6-phenyl methanol-1,2,4,5-tetrazine was synthesized as per protocol described elsewhere.^[24] Briefly, 4-cyanobenzylalcohol (0.51 g, 3.75 mmol), Ni(OTf)₂ (0.67 g, 1.88 mmol) and acetonitrile (1.97 mL, 37.6 mmol) were added in a 100 mL round flask, followed adding 60% NH₂NH₂·H₂O (12 mL), under N₂ flow. The mixture stirred at 60 °C for 24 h and allowed to cool to room temperature. Sodium nitrite (6.35 g, 92.0 mmol) in 14 mL water was slowly added to the reaction followed by careful addition of 5 M HCl until gas evolution ceased. (pH 3), in an ice bath with stirring. The product was extracted with ethyl acetate and organic phase was dried by sodium sulfate. The product was purified using silica column chromatography (EtOAc:heptane = 1:2.8) as a red solid. Yield = 0.33 g (41%); ¹H NMR (400 MHz, CDCl₃): δ = 3.08 (3H, s), 4.82 (2H, d), 7.57 (2H, d, *J* = 8 Hz), 8.55 ppm (2H, d, *J* = 8 Hz); ¹³C NMR (101 MHz, CDCl₃): δ = 21.1, 64.7, 127.4, 128.1, 130.9, 145.6, 163.9, 167.2 ppm.

Synthesis of 4-(6-methyl-1,2,4,5-tetrazin-3-yl)benzyl 4-(trifluoromethyl)benzoate (3)

4-(Trifluoromethyl)benzoic acid (0.27 g, 1.38 mmol), DMAP (0.01 g, 0.123 mmol), 2.5 mL DMF, DIC (0.18 mL, 1.18 mmol) and compound **2** (0.21 g, 0.98 mmol) were successively added and allowed to react at room temperature for 17 h. DMF was evaporated by rota-

tory evaporation under reduced pressure. The mixture was extracted with EtOAc and organic phase was washed with brine, dried with sodium sulfate and concentrated by rotatory evaporation to yield an oil, which was purified using silica column chromatography (EtOAc:heptane=1:4) to obtain a red solid. Yield=0.22 g (57%); ¹H NMR (400 MHz, CDCl₃): δ=3.11 (3H, s), 5.51 (2H, s), 7.67 (2H, d, *J*=8 Hz), 7.73 (2H, d, *J*=8 Hz), 8.22 (2H, d, *J*=8 Hz), 8.63 ppm (2H, d, *J*=8 Hz); ¹³C NMR (100 MHz, CDCl₃): δ=21.2, 66.5, 125.5, 128.3, 128.4, 128.7, 130.2, 131.9, 132.5, 133.1, 140.2, 163.8, 165.1, 167.4 ppm.

Synthesis of ((1*R*,2*S*,4*R*)-bicyclo[2.2.1]hept-5-en-2-yl)methyl 4-(trifluoromethyl)benzoate (4)

4-(Trifluoromethyl)benzoic acid (0.43 g, 2.25 mmol), DMAP (0.024 g, 0.190 mmol), 4 mL DMF, DIC (0.3 mL, 1.93 mmol) and ((1*R*,2*S*,4*R*)-bicyclo[2.2.1]hept-5-en-2-yl)methanol (0.19 mL, 1.61 mmol), were successively added in a 100 mL rounded flask and allowed to react for 16 h. DMF was removed using a rotary evaporator under reduced pressure. The mixture was extracted with EtOAc and organic phase was washed by brine, dried by sodium sulfate. The product was purified using silica column chromatography (EtOAc:heptane=1:4) as white solid. Yield=0.35 g (69%); ¹H NMR (400 MHz, CDCl₃): δ=1.23–1.40(4H, m), 1.88 (1H, m), 2.80(1H, s), 2.87(1H, s), 4.25(1H, m), 4.43(1H, m), 6.11(2H, m), 7.70 (2H, d, *J*=8 Hz), 8.16 ppm (2H, d, *J*=8 Hz); ¹³C NMR (100 MHz, CDCl₃): δ=29.6, 38.1, 41.6, 43.72, 45.0, 69.6, 122.3, 125.4, 130.0, 133.7, 134.52, 136.1, 137.0, 165.4 ppm.

Synthesis of ((1*S*,2*S*,4*S*)-bicyclo[2.2.1]hept-5-en-2-yl)methanol (5)

Commercially available mixture of *endo*- and *exo*- 5-norbornenecarboxylic acid, was subject to column chromatography (heptane:EtOAc=1:4) to obtain the *endo*-norbornene carboxylic acid only. (1*S*,2*S*,4*S*)-Bicyclo[2.2.1]hept-5-ene-2-carboxylic acid (206.6 mg, 1.5 mmol) was mixed with LiAlH₄ (113.5 mg, 3.0 mmol) in 20 mL dry ether for 2 h. The reaction was quenched with water and the organic product was extracted into ether followed by recovery of the product by evaporating the solvent under reduced pressure. Yield=0.15 g (81%). ¹H NMR (400 MHz, CDCl₃): δ=6.15 (dd, *J*=5.7, 3.0 Hz, 1H), 5.97 (dd, *J*=5.7, 2.9 Hz, 1H), 3.40 (dd, *J*=10.4, 6.5 Hz, 1H), 3.26 (dd, *J*=10.4, 8.9 Hz, 1H), 2.93 (s, 1H), 2.81 (s, 1H), 2.29 (ddt, *J*=9.2, 6.6, 4.5 Hz, 1H), 1.82 (ddd, *J*=11.6, 9.2, 3.8 Hz, 1H), 1.48–1.41 (m, 1H), 1.27 (d, *J*=8.2 Hz, 1H), 0.55–0.49 ppm (m, 1H).

Synthesis of ((1*S*,2*S*,4*S*)-bicyclo[2.2.1]hept-5-en-2-yl)methyl 4-(trifluoromethyl)benzoate (6)

4-(Trifluoromethyl)benzoic acid (0.43 g, 2.25 mmol), DMAP (0.024 g, 0.19 mmol), 4 mL DMF, DIC (0.3 mL, 1.93 mmol) and ((1*S*,2*S*,4*S*)-bicyclo[2.2.1]hept-5-en-2-yl)methanol, **5**, (0.19 mL, 1.61 mmol), were successively added in a 100 mL rounded flask, and allowed to react for 24 h. DMF was removed using a rotary evaporator under reduced pressure. The mixture was extracted with EtOAc and organic phase was washed by brine, dried by sodium sulfate. The product was purified using silica column chromatography (EtOAc:heptane=1:4) as white solid. Yield=0.14 g; (33%) ¹H NMR (400 MHz, CDCl₃): δ=8.17 (d, *J*=7.6 Hz, 2H), 7.72 (d, *J*=7.5 Hz, 2H), 6.22 (s, 1H), 6.01 (s, 1H), 4.21–4.07 (m, 1H), 3.96 (t, *J*=9.9 Hz, 1H), 2.98 (s, 1H), 2.87 (s, 1H), 2.57 (s, 1H), 1.93 (t, *J*=10.1 Hz, 1H), 1.51 (d, *J*=7.9 Hz, 1H), 1.32 (d, *J*=7.8 Hz, 1H), 0.67 ppm (d, *J*=10.2 Hz, 1H); ¹³C NMR (100 MHz, CDCl₃): δ=165.30, 137.81, 134.50, 134.18,

133.78, 132.07, 129.94, 125.35, 125.01, 125.01, 122.30, 68.91, 49.44, 43.99, 42.24, 37.89, 29.69, 28.98 ppm.

Preparation of phosphonic acid monolayers

Al slides (2×1 cm) were sonicated in hexane for 15 min followed by wiping with lint-free cotton swabs (Texwipe, NC, USA) to remove the polymer protection layer on top and remove any residual glue. The surfaces were chemically activated by immersion in 1:1 (v/v) 37% HCl–MeOH mixture for 5 min, followed by washing with copious amounts of water and 2-propanol. The activated surfaces were then immersed into N₂ filled vials of solution of octylphosphonic acid (1.5 mM) and 12-aminododecylphosphonic acid hydrochloride salt (0.5 mM) for “free” ME (*m*=7, *n*=3); hexadecylphosphonic acid (1.5 mM) and 6-aminohexylphosphonic acid hydrochloride salt (0.5 mM) for “buried” ME (*m*=1, *n*=11) mixture in 2-propanol, heated to 50 °C for 5 min, and then left undisturbed for 5 h at room temperature to obtain self-assembled mixed monolayers. Then surfaces were taken out and sonicated successively for 5 min with 2-propanol, acetone and CH₂Cl₂. The surfaces were finally cleaned with CH₂Cl₂, air dried and stored under N₂ atmosphere. From static water contact angle (SCA) measurements, it was found that the reaction was complete after 5 h, yielding monolayers with 28–30% C as determined by XPS. Substantially longer reaction times (16 h) contributed to the formation of undesirable multilayers (42–44% C1s in XPS wide scans).

Preparation of *exo*-norbornene terminated monolayers (M₂)

Amino-terminated monolayers (M₁) were stirred with 50 mM 1,1'-carbonyldiimidazole (CDI) solution in water for 1 h to yield acyl imidazole activated surfaces. These surfaces were immediately reacted with 50 mM *exo*-5-norbornene-2-methanol solution in DCE. This resulted in carbamate bond formation and covalent tethering of the *exo*-norbornene on the surface via carbamate bond in 16 h. The samples were sonicated and washed with copious amounts of CH₂Cl₂, dried and stored under nitrogen atmosphere.

Preparation of *endo*-norbornene terminated monolayers (M₃)

Amino-terminated monolayers (M₁) were stirred with 50 mM aqueous solution of 1,1'-carbonyldiimidazole (CDI) for 1 h to yield acyl imidazole-activated surfaces. These surfaces were immediately reacted with 50 mM *endo*-5-norbornene-2-methanol solution in DCE. This resulted in covalent tethering of the *endo*-norbornene on the surface via carbamate bond in 16 h. The samples were sonicated and washed with copious amounts of CH₂Cl₂, dried and stored under nitrogen atmosphere.

Preparation of tetrazine-terminated monolayers (M₄)

Amino-terminated monolayers (M₁) were stirred with 50 mM aqueous solution of 1,1'-carbonyldiimidazole (CDI) for 1 h to yield acyl imidazole-activated surfaces. These surfaces were immediately reacted with 50 mM (4-(6-methyl-1,2,4,5-tetrazin-3-yl)phenyl)methanamine, **1** solution in DCE. This resulted in covalent tethering of the tetrazine on the surface via urea bond in 16 h. The samples were sonicated and washed with copious amounts of CH₂Cl₂, dried and stored under nitrogen atmosphere.

General method for IEDDA reaction on *exo*-/*endo*-norbornene-terminated surface

Both free and buried *exo*-/*endo*-norbornene-terminated surfaces were reacted with a 4-(6-methyl-1,2,4,5-tetrazin-3-yl)benzyl 4-(trifluoromethyl)benzoate solution, **3** in DCE at 30 °C. The reaction was stirred at a constant speed using a magnetic bead and stirrer and all samples were loaded in a specially constructed Teflon holder to ensure rigorous reproducibility between samples. Samples were immersed into the solution for a set period of reaction time and immediately taken out and washed with copious amounts of CH₂Cl₂. The samples were further sonicated in CH₂Cl₂ to remove any physisorbed species for 15 min, dried under a dry nitrogen stream and stored for further analysis in a sealed vial.

General method for IEDDA reaction on tetrazine-terminated surface

Both "free" and "buried" tetrazine-terminated surfaces were reacted with ((1*R*,2*S*,4*R*)-bicyclo[2.2.1]hept-5-en-2-yl)methyl 4-(trifluoromethyl)benzoate [**4**, *exo*-norbornene tag molecule] or ((1*R*,2*R*,4*R*)-bicyclo[2.2.1]hept-5-en-2-yl)methyl 4-(trifluoromethyl) benzoate [**6**, *endo*-norbornene tag molecule] solution in DCE at 30 °C. The reaction was stirred at a constant speed using a magnetic bead and stirrer and all samples were loaded in a specially constructed Teflon holder to ensure rigorous reproducibility between samples. Samples were immersed into above said solution for a set period of reaction time and immediately taken out and washed with copious amounts of CH₂Cl₂. The samples were further sonicated in CH₂Cl₂ to remove any physisorbed species for 15 min, dried under a dry nitrogen stream and stored for further analysis in a sealed vial.

Acknowledgements

The authors thank the Netherlands Organization for Scientific Research for funding (ECHO project number 712.012.006), and Prof. Floris van Delft and Medea Kosian for stimulating discussions.

Conflict of interest

The authors declare no conflict of interest.

Keywords: cycloaddition · Diels–Alder reaction · mass spectrometry · reaction rates · organic surface chemistry

- [1] W. Tang, M. L. Becker, *Chem. Soc. Rev.* **2014**, *43*, 7013–7039.
 [2] F. Ehret, H. Wu, S. C. Alexander, N. K. Devaraj, *J. Am. Chem. Soc.* **2015**, *137*, 8876–8879.
 [3] C. D. Spicer, B. G. Davis, *Nat. Commun.* **2014**, *5*, 4740–4754.
 [4] E. M. Sletten, C. R. Bertozzi, *Angew. Chem. Int. Ed.* **2009**, *48*, 6974–6998; *Angew. Chem.* **2009**, *121*, 7108–7133.
 [5] a) S. P. Pujari, L. Scheres, A. T. M. Marcellis, H. Zuilhof, *Angew. Chem. Int. Ed.* **2014**, *53*, 6322–6356; *Angew. Chem.* **2014**, *126*, 6438–6474; b) H. C. Kolb, M. G. Finn, K. B. Sharpless, *Angew. Chem. Int. Ed.* **2001**, *40*, 2004–2021; *Angew. Chem.* **2001**, *113*, 2056–2075; c) J. Escorihuela, A. T. M. Marcellis, H. Zuilhof, *Adv. Mater. Interfaces* **2015**, *2*, 1500135.
 [6] a) K. Godula, D. Rabuka, K. T. Nam, C. R. Bertozzi, *Angew. Chem. Int. Ed.* **2009**, *48*, 4973–4976; *Angew. Chem.* **2009**, *121*, 5073–5076; b) B. Uzczyńska, T. Ratajczak, E. Frydrych, H. Maciejewski, M. Figlerowicz, W. T. Markiewicz, M. K. Chmielewski, *Lab on a Chip* **2012**, *12*, 1151–1156.
 [7] a) M. L. Blackman, M. Royzen, J. M. Fox, *J. Am. Chem. Soc.* **2008**, *130*, 13518–13519; b) N. K. Devaraj, R. Upadhyay, J. B. Haun, S. A. Hilderbrand, R. Weissleder, *Angew. Chem. Int. Ed.* **2009**, *48*, 7013–7016; *Angew. Chem.* **2009**, *121*, 7147–7150.
 [8] a) D. Wang, W. Chen, Y. Zheng, C. Dai, K. Wang, B. Ke, B. Wang, *Org. Biomol. Chem.* **2014**, *12*, 3950–3955; b) M. R. Karver, R. Weissleder, S. A. Hilderbrand, *Bioconjugate Chem.* **2011**, *22*, 2263–2270.
 [9] a) A.-C. Knall, M. Hollauf, C. Slugovc, *Tetrahedron Lett.* **2014**, *55*, 4763–4766; b) M. Vrabel, P. Kölle, K. M. Brunner, M. J. Gattner, V. López-Carrillo, R. de Vivie-Riedle, T. Carell, *Chem. Eur. J.* **2013**, *19*, 13309–13312.
 [10] P. Wang, Z. Na, J. Fu, C. Y. J. Tan, H. Zhang, S. Q. Yao, H. Sun, *Chem. Commun.* **2014**, *50*, 11818–11821.
 [11] a) N. K. Devaraj, R. Weissleder, S. A. Hilderbrand, *Bioconjugate Chem.* **2008**, *19*, 2297–2299; b) J. Schoch, M. Wiessler, A. Jäschke, *J. Am. Chem. Soc.* **2010**, *132*, 8846–8847; c) H. S. G. Beckmann, A. Niederwieser, M. Wiessler, V. Wittmann, *Chem. Eur. J.* **2012**, *18*, 6548–6554; d) O. Røling, A. Mardyukov, S. Lamping, B. Vonhoren, S. Rinnen, H. F. Arlinghaus, A. Studer, B. J. Ravoo, *Org. Biomol. Chem.* **2014**, *12*, 7828–7835.
 [12] R. Sen, D. Gahtory, R. R. Carvalho, B. Albada, F. L. van Delft, H. Zuilhof, *Angew. Chem. Int. Ed.* **2017**, *56*, 4130–4134; *Angew. Chem.* **2017**, *129*, 4194–4198.
 [13] a) N. S. Bhairamadgi, S. Gangarapu, M. A. Caipa Campos, J. M. J. Paulusse, C. J. M. van Rijn, H. Zuilhof, *Langmuir* **2013**, *29*, 4535–4542; b) J. Escorihuela, M. J. Banuls, R. Puchades, A. Maquieira, *Chem. Commun.* **2012**, *48*, 2116–2118.
 [14] a) R. Sen, J. Escorihuela, M. M. J. Smulders, H. Zuilhof, *Langmuir* **2016**, *32*, 3412–3419; b) R. Sen, J. Escorihuela, F. L. van Delft, H. Zuilhof, *Angew. Chem. Int. Ed.* **2017**, *56*, 3299–3303; *Angew. Chem.* **2017**, *129*, 3347–3351.
 [15] Y. Kwon, M. Mrksich, *J. Am. Chem. Soc.* **2002**, *124*, 806–812.
 [16] B. Rijksen, S. P. Pujari, L. Scheres, C. J. M. van Rijn, J. E. Baio, T. Weidner, H. Zuilhof, *Langmuir* **2012**, *28*, 6577–6588.
 [17] X. Fan, Y. Ge, F. Lin, Y. Yang, G. Zhang, W. S. Ngai, Z. Lin, S. Zheng, J. Wang, J. Zhao, J. Li, P. R. Chen, *Angew. Chem. Int. Ed.* **2016**, *55*, 14046–14050; *Angew. Chem.* **2016**, *128*, 14252–14256.
 [18] L. Törk, G. Jiménez-Osés, C. Doubleday, F. Liu, K. N. Houk, *J. Am. Chem. Soc.* **2015**, *137*, 4749–4758.
 [19] J. Yang, Y. Liang, J. Seckute, K. N. Houk, N. K. Devaraj, *Chem. Eur. J.* **2014**, *20*, 3365–3375.
 [20] Gaussian 09, Revision D.01, M. J. Frisch, G. W. Trucks, H. B. Schlegel, G. E. Scuseria, M. A. Robb, J. R. Cheeseman, G. Scalmani, V. Barone, B. Mennucci, G. A. Petersson, H. Nakatsuji, M. Caricato, X. Li, H. P. Hratchian, A. F. Izmaylov, J. Bloino, G. Zheng, J. L. Sonnenberg, M. Hada, M. Ehara, K. Toyota, R. Fukuda, J. Hasegawa, M. Ishida, T. Nakajima, Y. Honda, O. Kitao, H. Nakai, T. Vreven, J. A. Montgomery, Jr., J. E. Peralta, F. Ogliaro, M. J. Bearpark, J. Heyd, E. N. Brothers, K. N. Kudin, V. N. Staroverov, R. Kobayashi, J. Normand, K. Raghavachari, A. P. Rendell, J. C. Burant, S. S. Iyengar, J. Tomasi, M. Cossi, N. Rega, N. J. Millam, M. Klene, J. E. Knox, J. B. Cross, V. Bakken, C. Adamo, J. Jaramillo, R. Gomperts, R. E. Stratmann, O. Yazyev, A. J. Austin, R. Cammi, C. Pomelli, J. W. Ochterski, R. L. Martin, K. Morokuma, V. G. Zakrzewski, G. A. Voth, P. Salvador, J. J. Dannenberg, S. Dapprich, A. D. Daniels, Ö. Farkas, J. B. Foresman, J. V. Ortiz, J. Cioslowski, D. J. Fox, Gaussian, Inc., Wallingford, CT, USA, **2009**.
 [21] Y. Zhao, D. G. Truhlar, *Theor. Chem. Acc.* **2008**, *120*, 215–241.
 [22] a) F. Liu, R. S. Paton, S. Kim, Y. Liang, K. N. Houk, *J. Am. Chem. Soc.* **2013**, *135*, 15642–15649.
 [23] C. Gonzalez, H. B. Schlegel, *J. Phys. Chem.* **1990**, *94*, 5523–5527.
 [24] J. Yang, M. R. Karver, W. Li, S. Sahu, N. K. Devaraj, *Angew. Chem. Int. Ed.* **2012**, *51*, 5222–5225; *Angew. Chem.* **2012**, *124*, 5312–5315.

Manuscript received: July 6, 2017

Accepted manuscript online: July 13, 2017

Version of record online: August 23, 2017